JACC: CARDIOVASCULAR IMAGING VOL. 4, NO. 3, 2011

ISSN 1936-878X/$36.00
PUBLISHED BY ELSEVIER INC. DOI:10.1016/j.jcmg.2010.11.019

Contrast-Enhanced C-Arm CT Evaluation of Radiofrequency Ablation Lesions in the Left Ventricle

Erin E. Girard, MS,* Amin Al-Ahmad, MD,† Jarrett Rosenberg, PHD,‡ Richard Luong, BVSC, DACVP,§ Teri Moore, BS,‖ Günter Lauritsch, PHD,¶ Jan Boese, PHD,¶ Rebecca Fahrig, PHD‡

Palo Alto, California; Malvern, Pennsylvania; and Forchheim, Germany

OBJECTIVES The purpose of this study was to evaluate use of cardiac C-arm computed tomography (CT) in the assessment of the dimensions and temporal characteristics of radiofrequency ablation (RFA) lesions. This imaging modality uses a standard C-arm fluoroscopy system rotating around the patient, providing CT-like images during the RFA procedure.

BACKGROUND Both cardiac magnetic resonance (CMR) and CT can be used to assess myocardial necrotic tissue. Several studies have reported visualizing cardiac RFA lesions with CMR; however, obtaining CMR images during interventional procedures is not common practice. Direct visualization of RFA lesions using C-arm CT during the procedure may improve outcomes and circumvent complications associated with cardiac ablation procedures.

METHODS RFA lesions were created on the endocardial surface of the left ventricle of 9 swine using a 7-F RFA catheter. An electrocardiographically gated C-arm CT imaging protocol was used to acquire projection images during iodine contrast injection and after the injection every 5 min for up to 30 min, with no additional contrast. Reconstructed images were analyzed offline. The mean and SD of the signal intensity of the lesion and normal myocardium were measured in all images in each time series. Lesion dimensions and area were measured and compared in pathologic specimens and C-arm CT images.

RESULTS All ablation lesions (n = 29) were visualized and lesion dimensions, as measured on C-arm CT, correlated well with postmortem tissue measurements (linear dimensions: concordance correlation = 0.87; area: concordance correlation = 0.90. Lesions were visualized as a perfusion defect on first-pass C-arm CT images with a signal intensity of 95 HU lower than that of normal myocardium (95% confidence interval: −111 HU to −79 HU). Images acquired at 1 and 5 min exhibited an enhancing ring surrounding the perfusion defect in 24 lesions (83%).

CONCLUSIONS RFA lesion size, including transmurality, can be assessed using electrocardiographically gated cardiac C-arm CT in the interventional suite. Visualization of RFA lesions using cardiac C-arm CT may facilitate the assessment of adequate lesion delivery and provide valuable feedback during cardiac ablation procedures. (J Am Coll Cardiol Img 2011;4:259–68) © 2011 by the American College of Cardiology Foundation

From the *Department of Bioengineering, Stanford University, Palo Alto, California; †Department of Medicine, Stanford University, Palo Alto, California; ‡Department of Radiology, Stanford University, Palo Alto, California; §Department of Comparative Medicine, Stanford University, Palo Alto, California; ‖Siemens Medical Solutions Inc., Malvern, Pennsylvania; and ¶Siemens AG, Healthcare Sector, Forchheim, Germany. This project is supported by NIH grant R01 HL087917 (Bethesda, Maryland), Siemens Medical Solutions (Malvern, Pennsylvania), Medtron AG (Saarbruecken, Germany), and the Lucas Foundation (Stanford, California). Drs. Fahrig and Al-Ahmad receive research support from Siemens AG, Healthcare Sector. Ms. Moore is an employee of Siemens Medical Solutions, Inc., and Drs. Lauritsch and Boese are employees of Siemens AG, Healthcare Sector. All other authors have reported that they have no relationships to disclose.

Manuscript received November 16, 2010, accepted November 22, 2010.

JACC: CARDIOVASCULAR IMAGING, VOL. 4, NO. 3, 2011
MARCH 2011:259–68

Radiofrequency ablation (RFA) has emerged as an important nonpharmacological strategy in the treatment of both supraventricular and ventricular arrhythmias (1,2). The main challenges of RFA are the ability to accurately map cardiac arrhythmias and, once mapped, the delivery of an adequate lesion to the selected site. Lesion formation depends on multiple factors that affect the delivery of radiofrequency (RF) current to the tissue, including contact and force of the catheter on the tissue and catheter tip cooling in the blood volume. Currently, during RF lesion creation, surrogates of lesion quality are assessed, such as temperature at the catheter tip, the amount of power delivered and delivery time, and the change in impedance during lesion delivery. Despite monitoring these parameters, failure to deliver an adequate lesion remains 1 cause of failed catheter ablation procedures.

Three-dimensional (3D) cardiac images can be obtained during an interventional procedure using C-arm computed tomography (CT), an imaging modality that uses a standard C-arm fluoroscopy system rotating around the patient (3). We hypothesize that with the addition of contrast, necrotic tissue can be visualized in C-arm CT images based on the different wash-in and wash-out kinetics of iodine in necrotic tissue compared with healthy myocardium. Cardiac C-arm CT has high spatial resolution and can be performed without altering the fundamental clinical work flow because standard C-arm fluoroscopy equipment is used. Most important, cardiac C-arm CT accurately represents the anatomic and hemodynamic state of the patient in the interventional suite at the time of the RFA procedure.

ABBREVIATIONS AND ACRONYMS

CMR = cardiac magnetic resonance
CT = computed tomography
3D = 3-dimensional
LV = left ventricle
RF = radiofrequency
RFA = radiofrequency ablation
VT = ventricular tachycardia

In this study, we examined the ability of contrast-enhanced cardiac C-arm CT to visualize lesions delivered in the porcine left ventricle (LV). We aimed to: 1) quantify lesion dimensions and area on C-arm CT images; 2) correlate C-arm CT lesion dimensions and area with pathological measurements; and 3) describe the contrast kinetics of ablated myocardial tissue using a time series of C-arm CT images.

METHODS

Animal model. Stanford University's Administrative Panel on Laboratory Animal Care approved the protocol for this in vivo study. Nine female Yorkshire swine (weighing 49 to 55 kg) were anesthetized intramuscularly with 5 to 7 mg/kg Telazol (tiletamine HCl and zolazepam HCl) (Fort Dodge Animal Health, Fort Dodge, Iowa) and 0.05 mg/kg atropine and were maintained on 80% oxygen and 2.0% to 3.5% isoflurane with a respirator. Venous and arterial femoral access was established using percutaneous puncture for the purpose of hemodynamic monitoring, administration of medications, and contrast injections.

An RF generator (EPT 1000, Boston Scientific, Natick, Massachusetts) and a 7-F RFA catheter (4-mm solid tip Blazer, Boston Scientific) were used to create ablation lesions on the endocardial surface of the LV. RF catheter access was via the femoral artery. Two to 5 lesions were created using standard fluoroscopy to guide the ablation catheter to various locations throughout the left ventricular cavity. The RF generator used a power of 50 W for 30 s, and tissue temperature and impedance were monitored to ensure conductivity. Amiodarone (150 to 300 mg total) was administered as needed to prevent tachyarrhythmias.

C-arm CT image acquisition. Cardiac C-arm CT is based on rotating a C-arm angiography system in forward and backward sweeps, triggering each sweep based on the electrocardiogram (syngo DynaCT Cardiac, Siemens AG, Healthcare Sector, Erlangen, Germany) (Fig. 1) (3,4). All C-arm CT projection images were acquired with electrocardiography for retrospective gating using 4 sweeps of 5 s each for a total of 992 projection images (249 projection images/sweep).

Image acquisition began 30 min after the completion of the last RFA to ensure hemodynamic stability of the animal before contrast administration and multiple breath holds. The first-pass C-arm CT began after a 42-s peripheral injection of iodinated contrast (Omnipaque 350 mg/ml, GE Healthcare, Princeton, New Jersey). The contrast was delivered through a 6-F pigtail catheter placed in the inferior vena cava using a power injector (Medtron, Saarbrücken, Germany) programmed for a 2-phase protocol of 150 ml (4 ml/s) of iodinated contrast followed by a 16-ml (4 ml/s) saline solution flush. A series of C-arm CT images were acquired with no additional contrast at 1 min and every 5 min from 5 to 30 min.

The entrance dose at the detector for all scans was 1.2 μGy per projection, and a tube voltage of 90 kV was used for the first-pass and 1-min image acquisition; all subsequent images in the time series were acquired with 70 kV. Breathing was held at

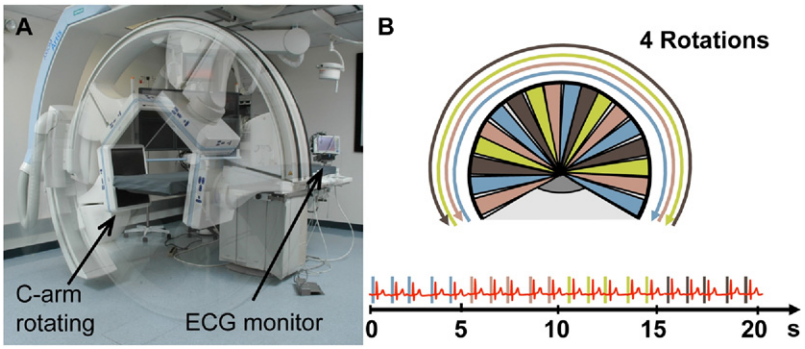

Figure 1. The C-Arm CT System With Multiple Sweeps and ECG Gating

(A) The C-arm rotates 200° about the field of view with integrated electrocardiographic (ECG) monitoring. **(B)** Schematic illustrating how views from multiple sweeps are chosen from a given cardiac phase to fill the 200° required for a 3-dimensional reconstruction. CT = computed tomography.

inspiration for the duration of each image acquisition, approximately 24 to 30 s.

Postmortem tissue examination. After the imaging protocol was completed, the animals were euthanized with a Beuthanasia solution (1 ml/10 lb intravenous dose) (D Special, Animal Health Corp., Union, New Jersey). The heart was excised, and the lesions were sectioned from the heart and placed in a 1% solution of 2,3,5-triphenyltetrazolium chloride at 37° C for 20 min. The tissue was then placed in 10% neutral buffered formalin for a minimum of 48 h. The lesion measurements were performed on 2,3,5-triphenyltetrazolium chloride–stained formalin-kept specimens after 48 h. Lesion size was measured on 3 perpendicular dimensions: the 2 diameters of the lesion on the endocardial wall and the transmurality. High-resolution digital photographs were taken of the transmural extent of the lesion and used for planimetry of the necrotic region. The tissue was subsequently processed for routine histological analysis using hematoxylin and eosin staining.

C-arm CT image analysis. Electrocardiographically gated C-arm CT images were reconstructed at the end of ventricular diastole (80% R-R interval) using a 3D Feldkamp reconstruction algorithm with correction for scatter, beam hardening, truncation, and ring artifact, as detailed previously (3). The 3D volume dimension was 512 × 512 × 380 with an isotropic voxel resolution of 0.50 mm. Measurements were performed using an offline workstation and image analysis toolkit (syngo X Workplace, Siemens AG, Healthcare Sector). The desired slices of the reconstructed volumes were visualized as multiplanar reformatted images with a 0.5-mm slice thickness. The extent of the lesion was delineated on the first-pass image as a perfusion defect compared with the enhanced, normal myocardium. Image slices corresponding to pathology were used to measure the 3 perpendicular dimensions and for planimetry of the lesion area.

The lesion contrast over time was analyzed by measuring the mean intensity in Hounsfield units in 3 regions of interest: the lesion core, the periphery of the lesion, and a remote area of nonablated myocardium (average region of interest size: 6-mm^2 lesion core and periphery, 17-mm^2 myocardium). Figure 2 illustrates the expected enhancement patterns for the first-pass image and late images (5,6). The region of healthy myocardium was chosen within 2 cm of the ablation location so that contrast perfusion and image artifact levels would be similar.

Statistical analysis. Agreement between C-arm CT and pathological measurements was assessed for the 3 dimensions and the area by means of concordance correlations and Bland-Altman 95% limits of agreement. Differences over time in intensity between lesion and myocardium and between enhancing ring and myocardium were assessed with hierarchical mixed-effects longitudinal regression to account for the clustering of observations within animal and across time. The signal-intensity curves show the mean and 95% confidence interval (CI) for the difference in signal intensity of the lesion and myocardium at each point in time; lines are from the fitted regression models. Values of $p < 0.05$ were considered significant. All statistical analyses were done with Stata Release version 9.2 (StataCorp LP, College Station, Texas).

JACC: CARDIOVASCULAR IMAGING, VOL. 4, NO. 3, 2011
MARCH 2011:259–68

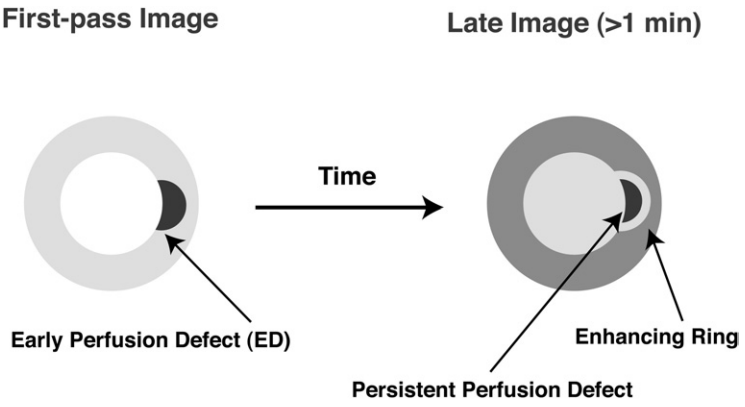

Figure 2. Schematic Illustrating the Contrast Kinetics in the Myocardium and Cavity

Radiofrequency ablation lesions exhibit an early perfusion defect on the first-pass image due to a prevention of contrast perfusion to the necrotic tissue. The signal intensity around the periphery of the lesion may increase to more than that of normal myocardium because of contrast accumulation (enhancing ring), whereas the core of the lesion remains a persistent perfusion defect.

RESULTS

Two to 5 lesions per swine, for a total of 29 lesions, were created in the myocardium of 9 swine. During RF energy delivery, the tissue impedance ranged from 70 to 130 Ω, and the tissue temperature reached higher than 50°C and not higher than 65° C for all lesions, ensuring tissue necrosis. Two swine were successfully defibrillated for ventricular fibrillation during RFA. All lesions were visualized on both gross inspection of pathology specimens and the C-arm CT images. Because the study was not blinded for lesion detection, the C-arm CT images were available during the pathological examination, and the lesions identified on C-arm CT correlated well with the locations in 2,3,5-triphenyltetrazolium chloride–stained tissue. The lesions were located throughout the LV as follows: 10 anterior, 6 posterior, 6 septal, 7 lateral and 9 basal, 11 mid-ventricle, and 9 apical.

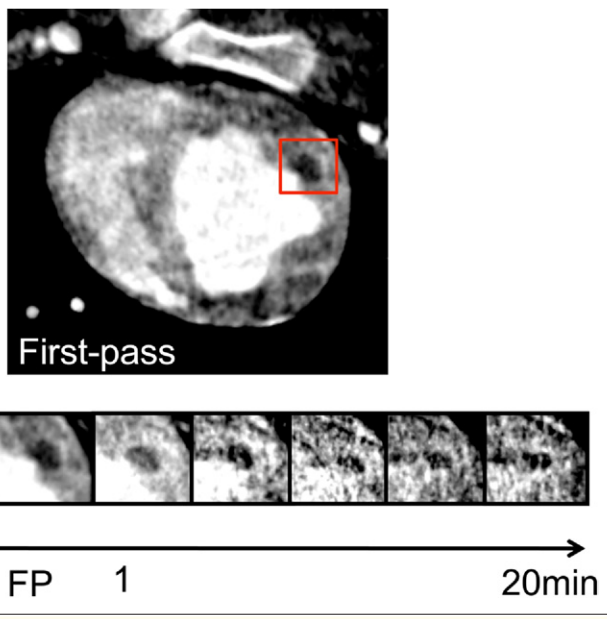

Figure 3. RFA Lesion Imaged From FP to 20 Min

The area outlined in **red** is shown for the same image slice over time and illustrates the perfusion defect and the enhancing ring at the periphery. First-pass (FP) image gray-scale window. Window width = 290 HU, contrast = 165 HU.

Lesion visualization with sequential C-arm CT imaging (time series). All RFA lesions were characterized in the first-pass image (time 0 min) by a hypoenhanced region, due to a perfusion defect, with the lesion clearly delineated from enhanced normal myocardium. Some peripheral enhancement was seen in 22 of the lesions (76%) on the first-pass image. Images acquired at 1 and 5 min more clearly showed the peripheral enhancement as a ring surrounding the perfusion defect and 24 of the lesions (83%) had peripheral enhancement. The characteristics of the perfusion defect and ring of enhancement were consistent in sequential images acquired 1 to 20 min after contrast administration, as illustrated in Figure 3, although the overall contrast of the lesion decreased and the size of the perfusion defect decreased over time as the enhancing ring increased, possibly due to the passive diffusion of contrast toward the core of the lesion. The signal intensity in normal myocardium decayed over time ($p < 0.001$), whereas the intensity of the perfusion defect remained essentially constant ($p = 0.048$), at a lower level than that of myocardium ($p < 0.001$) (Fig. 4A). The signal intensity in both normal

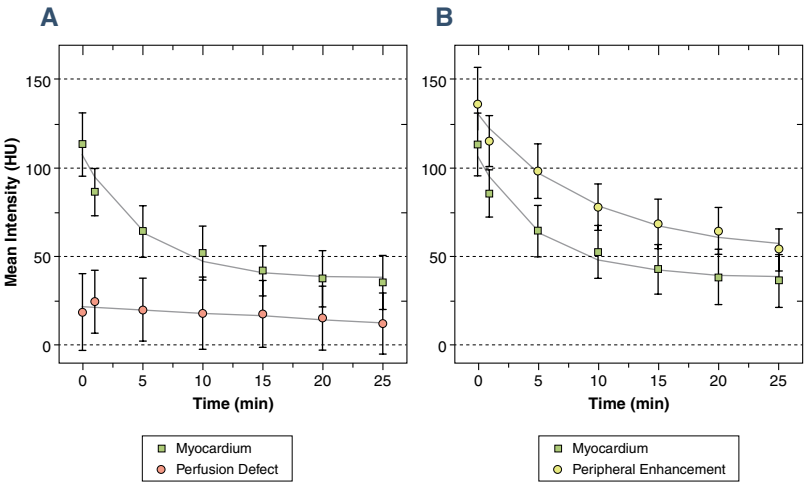

Figure 4. Myocardial and Lesion Signal Intensity as a Function of Time

The perfusion defect remains constant and with a lower intensity than normal myocardium **(A)**. The enhanced region around the periphery has a signal intensity consistently higher than that of normal myocardium, although decreasing over time **(B)**.

myocardium and enhancing ring decayed over time ($p < 0.001$), with ring intensity always higher than myocardium ($p < 0.001$) (Fig. 4B).

The contrast of the lesion compared with normal myocardium is shown in Figure 5A by comparing the signal intensity difference of the perfusion defect and enhancing ring with normal myocardium. The positive values are indicative of enhancement, and the negative values illustrate a perfusion defect compared with normal myocardium. The perfusion defect had maximum mean signal intensity less than that of normal myocardium in the first-pass image of −95 HU (95% CI: −111 to −79 HU), whereas the maximum intensity difference between the enhancing ring and normal myocardium occurred at 5 min with a difference of +37 HU (95% CI: 26 to 48 HU). Images acquired at 1 min nicely contrast the perfusion defect and the enhancing ring (Fig. 5B).

Lesion visualization with pathology. Gross examination of the RFA lesions revealed consistent observations in all locations and consisted of 2 distinct concentric regions: a central, round to spherical delineated core of pale tan tissue surrounded by a

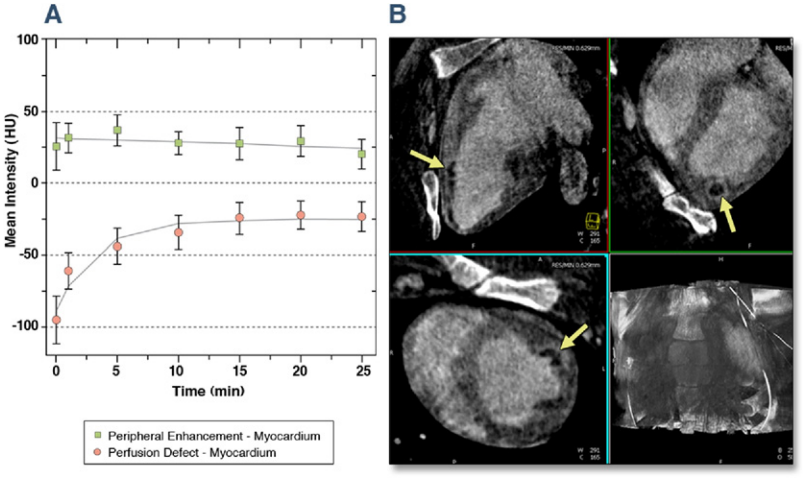

Figure 5. Comparison of the Lesion and Normal Myocardium

Lesion core and the enhancing ring compared with normal myocardium **(A)**. The **yellow arrows (B)** point to the same lesion in 3 perpendicular slices in an image acquired at 1 min post-contrast. Grayscale window width = 290 HU, contrast = 165 HU.

JACC: CARDIOVASCULAR IMAGING, VOL. 4, NO. 3, 2011
MARCH 2011:259–68

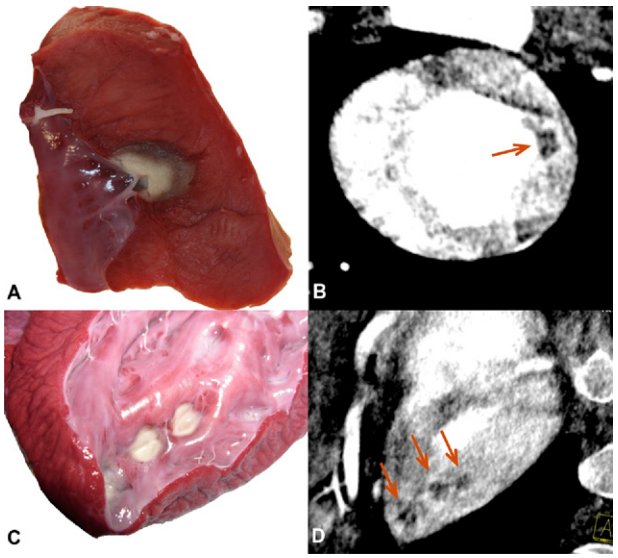

Figure 6. Pathological Specimens and the Corresponding First-Pass C-Arm CT Images

Pathological specimens **(A, C)** and the corresponding first-pass C-arm computed tomography (CT) images **(B, D)** of radiofrequency ablation lesions (**orange arrows**). Grayscale window width = 150 HU, C = 50 HU for **(B)** and window width = 250 HU, contrast = 115 HU for **(D)**.

peripheral, thin, dark, border zone of uniform, dark red tissue (Figs. 6A and 6C). These concentric regions were observable both superficially on the endocardial surfaces and on cut surfaces of the myocardium. The first-pass C-arm CT images corresponding to the pathological specimens are shown in Figures 6B and 6D.

Microscopic examination of the hematoxylin and eosin–stained sections of the RFA lesions revealed that the core of central pallor was myocardium undergoing peracute coagulation necrosis with scattered and random sarcoplasmic changes of these myocytes (Fig. 7A). The border zone contained peracute necrotic cardiomyocytes that were separated from each other by interstitial edema and hemorrhage (Fig. 7B), unlike the regularized pattern of healthy myocardium (Fig. 7C). The endocardial surface overlying the RFA lesions was microscopically denuded of viable endothelium.

In summary, gross and microscopic pathological findings are consistent with early heat-induced necrosis of myocardial tissue.

Correlation of first-pass C-arm CT images and pathology. Visual inspection of the lesions on first-pass C-arm CT images showed size and shape comparable to those of the gross pathological RFA lesions (Fig. 6). The largest diameter, its perpendicular, and transmural dimensions were successfully measured on the endocardial wall for all lesions on the first-pass C-arm CT image and pathological specimens. Lesion dimensions (2 perpendicular and 1 transmural) on pathology ranged between 2.5 and 10.5 mm (mean 5.9 mm) and correlated well with measurements of the perfusion defect on first-pass C-arm CT (concordance correlation = 0.87) with a mean difference of 0.09 ± 1.04 mm. The Bland-Altman 95% limits of agreement are −1.94 to 2.12 mm, and the bias and precision are constant across the measured range (Fig. 8A). Lesion areas ranged from 14.7 mm^2 to 60.1 mm^2 (mean 28.9 mm^2); Figure 8B shows the Bland-Altman distribution with 95% limits of agreement of −12.21 mm^2 to 10.79 mm^2. Lesion area on pathology correlated well with measurements on C-arm CT (concordance correlation = 0.90) with a mean difference of −0.71 ± 5.86 mm^2.

DISCUSSION

Main findings. In this study, we showed for the first time the ability to visualize RFA lesions and accurately measure their size during an RFA procedure using cardiac C-arm CT. The direct assessment of

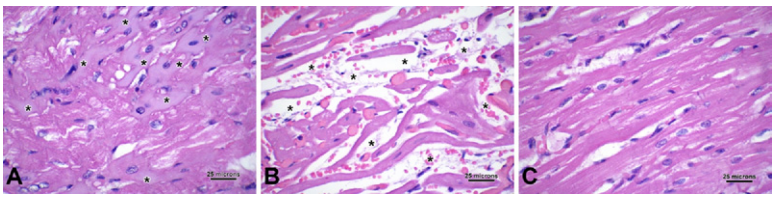

Figure 7. Hematoxylin and Eosin–Stained Sections of an RFA Lesion

Histopathologic examination distinguished the core of the lesion **(A)** from a peripheral border zone **(B)** before transitioning to healthy myocardium **(C)**. The core of the lesion **(A)** consists of some cardiac myocytes undergoing early coagulation necrosis (*, with loss of sarcoplasmic cross-striations) with the retention of some normal cardiac myocytes in between. The border zone **(B)** is characterized by interstitial edema and hemorrhage (*) that separates the necrotic and normal cardiac myocytes. Healthy myocardium **(C)** has normal cardiac myocytes that contain regular sarcoplasmic cross-striations. The hematoxylin and eosin stain is shown at a magnification of 600. RFA = radiofrequency ablation.

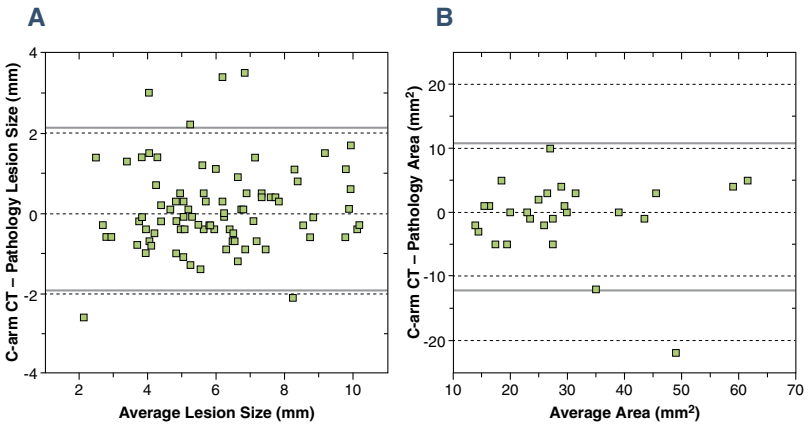

Figure 8. Bland-Altman Plots of Lesion Dimensions and Lesion Area

Bland-Altman plots showing the correlation of the lesion dimensions **(A)** and the lesion area **(B)**. CT = computed tomography.

lesion creation is not possible with other currently available tools, and cardiac C-arm CT could be a direct visual method for assessing the success of an ablation procedure. Procedure success relies on creating lesions of sufficient size and transmurality, which is inhibited by poor tissue contact with the ablation catheter and insufficient power delivery to the tissue (2).

Imaging RFA lesions. Currently, intracardiac echocardiography is being investigated to assess lesion dimensions during RFA procedures. Khoury et al. (7) reported that contrast-enhanced intracardiac echocardiography can visualize and accurately quantify the depth and diameter of RFA lesions in the dog LV. Intracardiac echocardiography is real-time, nonionizing, and routinely used during RFA procedures for guidance, but requires multiple injections of contrast microbubbles into each of the coronary arteries and has a limited field of view that is not capable of visualizing the entire chamber (or region) of interest.

Several pre-clinical studies have reported visualizing cardiac RFA lesions with gadolinium-enhanced or noncontrast-enhanced CMR (8–11). Our method of contrast enhanced C-arm CT is similar to the gadolinium-enhanced CMR visualization of lesions. In the study by Dickfeld et al. (8), lesions were visualized and measured at 3 distinct phases after gadolinium administration where the lesion appeared as: 1) a signal void at 1 min; 2) a peripheral enhancement at 15 to 45 min; and 3) fully enhanced at 98 ± 21 min. The lesion size measured at phase 1 (signal void) correlated best with pathological lesion size. Iodine contrast is similar in molecular weight to gadolinium (approximately 800 Da) and should diffuse comparably. Our results similarly showed primarily a contrast void on the first image, followed by peripheral enhancement in later images. However, the sensitivity of C-arm CT is not sufficient to permit measurement of lesion size at later time points, and the best contrast for lesion visualization was found during the first-pass and 1-min images.

CMR is nonionizing and has good contrast-to-noise ratio for detecting low-contrast lesions, and recently the feasibility of CMR-compatible electrophysiology systems has been shown for 3D visualization and real-time guidance (12,13). However, CMR-guided interventional procedures are not yet common practice because the technology requires the procedure to be performed in a closed-bore system with nonferromagnetic devices, including monitoring and ablation equipment, and because of concerns for compatibility with implanted devices and heating (12,13). C-arm CT provides a familiar clinical workflow as well as real-time fluoroscopy, 3D volumetric imaging, and good patient access.

Imaging necrotic tissue with CT. To our knowledge, there are no reports of CT or C-arm CT imaging of cardiac RFA lesions, but there is significant experience with CT for imaging necrotic tissue from other noncardiac RFA procedures and from myocardial infarction (6,14–17). The C-arm CT characteristics that we observed for RFA lesions in the myocardium are comparable to CT findings in liver RFA. In CT images of the liver acquired 30 min after RFA, a successfully ablated region presents as a hypoenhancement, due to coagulation necrosis, on an arterial phase CT (17) with a peripheral ring of enhancement in 79% of the cases (6). At 1-week

post-RFA, the contrast between normal liver and an RFA lesion is approximately −65 HU (18), which is comparable to the contrast between ablated and normal myocardium that we observed in images acquired 1 min after contrast administration (−68.2 ± 29.8 HU).

In the myocardium, contrast-enhanced CT can visualize perfusion abnormalities due to myocardial infarction (19). Typically, first-pass images acquired during the injection of contrast will exhibit an early perfusion defect correlating with the region of infarction with a signal intensity of at least 60 HU less than that of healthy myocardium (5,16), which is similar to the imaging characteristics that we observed for RFA lesions. CT (and CMR) can visualize and define 3D scar anatomy and potentially elucidate scar-related ventricular tachycardia (VT) circuits (20,21) but also presents the potential difficulty of imaging lesions in scar areas with impeded perfusion. Further work is required to establish that previous scar tissue and RFA lesions near the VT substrate can be visualized using C-arm CT.

C-arm CT image quality. Although the tradeoff between image quality and dose is well understood for clinical CT, C-arm CT images have additional artifacts due to beam hardening, scatter, truncation, motion, and cone beam that are detrimental to image quality. In this study, we did not work to optimize dose because the first purpose of this study was to demonstrate that lesions could be seen and accurately measured using our new protocol. Thus, we chose a higher dose (1.2 μGy per projection at 70 or 90 kV), high-contrast-burden (3 mg iodine/kg) protocol to minimize the artifact and maximize the low-contrast detectability. The lower tube voltage also increased the contrast between healthy, nonenhanced myocardium and the accumulated contrast in necrotic tissue (22,23).

Although our protocol was not optimized for dose, we can compare the dose from C-arm CT to clinical CT and place the imaging dose in the context of electrophysiology procedures. Absorbed dose was measured during one of our studies using 5 dosimeters (Dxposure Radiology Dosimetry System, high-sensitivity MOSFET dosimeters, Best Medical Canada, Ottawa, Ontario, Canada), 4 placed just under the skin circumferentially and 1 placed in the esophagus, yielding an effective dose of 27.2 mSv. A recent study measured dose during C-arm CT imaging of the relatively stationary left atrium using a single-sweep protocol in 42 patients, providing an estimate of 5.5 mSv (24), from which a 4-sweep dose of 22 mSv can be estimated for our protocol, in approximate agreement with our measured dose. Another cardiac C-arm CT study using a lower dose clinical protocol (0.54 μGy per projection at 70 kV) measured doses of 10.88 mSv in an anthropomorphic phantom (25). For comparison, the typical effective dose for multidetector row CT angiography ranges from 6.7 to 13.0 mSv (26) and electrophysiology procedures average from 1.5 to 49.8 mSv (27,28), with a large variance depending on length and type of procedure.

Future investigations with the aim of optimizing image quality and reducing dose should be conducted. For example, scatter and dose can be minimized by tight collimation in the axial direction and use of a wedge filter, whereas image quality could be further improved using post-processing methods for beam-hardening correction. The 4 × 5 s acquisition protocol was chosen for the narrow temporal window reconstructed, which minimizes motion-related blurring and streak artifacts. Dose could be reduced by decreasing the number of projection images acquired (e.g., fewer sweeps or prospective electrocardiographically triggered projections), an approach that has already shown a dramatic decrease in dose for helical CT angiography (29). Cardiac C-arm CT is a new imaging modality and hardware improvements such as an increased rotation speed of the C-arm and new software reconstruction and correction algorithms should allow visualization of RFA lesions with a lower dose protocol.

Study limitations. The study design only allowed for visualization and quantification of the lesions at a single, acute end point. C-arm CT imaging began 30 min after the last lesion and approximately 90 min after the first lesion. In light of VT ablation procedures, which can be several hours long, C-arm CT imaging should be evaluated at several time points after lesion creation, although the lesions should still have considerable hemorrhage and edema in that time frame. From a clinical perspective, it is also important to assess chronic lesions to determine how much of an ablative margin is necessary so that multiple ablation lesions remain contiguous over the course of tissue healing and remodeling. Additionally, acute RFA lesion visualization should be assessed in the presence of chronic myocardial scar tissue. Last, lesion measurement was performed after 48 h of fixation, and shrinking of the lesions during the fixation process was not accounted for in the measurements.

Clinical implications. Direct visualization and transmural assessment of adequate lesion delivery may circumvent some factors that complicate cardiac ablation procedures. For example, in RFA for VT, the following difficulties could be aided by imaging ablation lesions: a VT zone that is intramural or epicardial and not just subendocardial; the presence of several re-entrant circuits; difficulty with mapping; and a potentially large region of myocardial infarction (1,2). Also, because cardiac C-arm CT volumes accurately represent the state of the patient at the time of the intervention, the images could easily be merged and registered with tracking systems for defining the ablation strategy and image guidance during the procedure. This has initially been demonstrated using contrast-enhanced CT images of myocardial scar to define the ablation strategy and guide the VT ablation procedure (21), but has the disadvantage that the pre-procedural image does not represent the current state of the patient.

CONCLUSIONS

Electrocardiographically gated C-arm CT provides good visualization of the spatial extent of RFA lesions within a high-resolution cardiac image depicting the anatomy at the time of procedure. The primary advantage of electrocardiographically gated cardiac C-arm CT is that it can be used in the interventional suite with minimal disruption to the clinical workflow, without moving the patient, and may provide feedback or an assessment of the success of an ablation procedure before the patient leaves the interventional suite. This is the first study to demonstrate the visualization and spatial characterization of RFA lesions using cardiac C-arm CT.

Acknowledgments

The authors thank Wendy Baumgardner, RVT, LATg, and Pamela Hertz, RVT, for their assistance with the animal care and Michelle Lai, BA, for her assistance with postmortem tissue examination.

Reprint requests and correspondence: Erin Girard, Stanford University, 1201 Welch Road, Palo Alto, California 94304. *E-mail: egirard@stanford.edu.*

REFERENCES

1. Stevenson WG, Soejima K. Catheter ablation for ventricular tachycardia. Circulation 2007;115:2750–60.
2. Wang PJ. Ventricular Arrhythmias and Sudden Cardiac Death. Malden, MA: Blackwell Futura, 2008.
3. Lauritsch G, Boese J, Wigstrom L, Kemeth H, Fahrig R. Towards cardiac C-arm computed tomography. IEEE Trans Med Imaging 2006;25:922–34.
4. Al-Ahmad A, Wigström L, Sandner-Porkristl D, et al. Time-resolved three-dimensional imaging of the left atrium and pulmonary veins in the interventional suite—a comparison between multisweep gated rotational three-dimensional reconstructed fluoroscopy and multislice computed tomography. Heart Rhythm 2008;5:513–9.
5. Koyama Y, Mochizuki T, Higaki J. Computed tomography assessment of myocardial perfusion, viability, and function. J Magn Reson Imaging 2004;19:800–15.
6. Lim HK, Choi D, Lee WJ, et al. Hepatocellular carcinoma treated with percutaneous radio-frequency ablation: evaluation with follow-up multiphase helical CT. Radiology 2001;221:447–54.
7. Khoury DS, Rao L, Ding C, et al. Localizing and quantifying ablation lesions in the left ventricle by myocardial contrast echocardiography. J Cardiovasc Electrophysiol 2004;15:1078–87.
8. Dickfeld T, Kato R, Zviman M, et al. Characterization of radiofrequency ablation lesions with gadolinium-enhanced cardiovascular magnetic resonance imaging. J Am Coll Cardiol 2006;47:370–8.
9. Dickfeld T, Kato R, Zviman M, et al. Characterization of acute and subacute radiofrequency ablation lesions with nonenhanced magnetic resonance imaging. Heart Rhythm 2007;4:208–14.
10. Lardo AC, Cordeiro MA, Silva C, et al. Contrast-enhanced multidetector computed tomography viability imaging after myocardial infarction: characterization of myocyte death, microvascular obstruction, and chronic scar. Circulation 2006;113:394–404.
11. Schmidt EJ, Mallozzi RP, Thiagalingam A, et al. Electroanatomic mapping and radiofrequency ablation of porcine left atria and atrioventricular nodes using magnetic resonance catheter tracking. Circ Arrhythm Electrophysiol 2009;2:695–704.
12. Lardo AC, McVeigh ER, Jumrussirikul P, et al. Visualization and temporal/spatial characterization of cardiac radiofrequency ablation lesions using magnetic resonance imaging. Circulation 2000;102:698–705.
13. Nazarian S, Kolandaivelu A, Zviman MM, et al. Feasibility of real-time magnetic resonance imaging for catheter guidance in electrophysiology studies. Circulation 2008;118:223–9.
14. Davenport MS, Caoili EM, Cohan RH, et al. MRI and CT characteristics of successfully ablated renal masses: imaging surveillance after radiofrequency ablation. AJR Am J Roentgenol 2009;192:1571–8.
15. Habis M, Capderou A, Sigal-Cinqualbre A, et al. Comparison of delayed enhancement patterns on multislice computed tomography immediately after coronary angiography and cardiac magnetic resonance imaging in acute myocardial infarction. Heart 2009;95:624–9.
16. Lessick J, Dragu R, Mutlak D, et al. Is functional improvement after myocardial infarction predicted with myocardial enhancement patterns at multidetector CT? Radiology 2007;244:736–44.

17. Park MH, Rhim H, Kim YS, Choi D, Lim HK, Lee WJ. Spectrum of CT findings after radiofrequency ablation of hepatic tumors. Radiographics 2008;28:379–90, discussion 90–2.
18. Berber E, Foroutani A, Garland AM, et al. Use of CT Hounsfield unit density to identify ablated tumor after laparoscopic radiofrequency ablation of hepatic tumors. Surg Endosc 2000; 14:799–804.
19. Ko SM, Kim YW, Han SW, Seo JB. Early and delayed myocardial enhancement in myocardial infarction using two-phase contrast-enhanced multidetector-row CT. Korean J Radiol 2007;8:94–102.
20. Ashikaga H, Sasano T, Dong J, et al. Magnetic resonance-based anatomical analysis of scar-related ventricular tachycardia: implications for catheter ablation. Circ Res 2007;101:939–47.
21. Bello D, Kipper S, Valderrabano M, Shivkumar K. Catheter ablation of ventricular tachycardia guided by contrast-enhanced cardiac computed tomography. Heart Rhythm 2004;1: 490–2.
22. Mahnken AH, Bruners P, Muhlenbruch G, et al. Low tube voltage improves computed tomography imaging of delayed myocardial contrast enhancement in an experimental acute myocardial infarction model. Invest Radiol 2007;42:123–9.
23. Fahrig R, Dixon R, Payne T, Morin RL, Ganguly A, Strobel N. Dose and image quality for a cone-beam C-arm CT system. Med Phys 2006;33: 4541–50.
24. Wielandts JY, Smans K, Ector J, De Buck S, Heidbuchel H, Bosmans H. Effective dose analysis of three-dimensional rotational angiography during catheter ablation procedures. Phys Med Biol 2010;55:563–79.
25. Das M, Hohl C, Boese J, Strobel N, Banckwitz R, Muehlenbruch G. Angiographic CT: measurement of patient dose. Abstract presented at: Radiological Society of North America 94th Scientific Assembly and Annual Meeting; December 1, 2008; Chicago, Illinois [abstract SSE25-06:414].
26. Hunold P, Vogt FM, Schmermund A, et al. Radiation exposure during cardiac CT: effective doses at multidetector row CT and electron-beam CT. Radiology 2003;226:145–52.
27. Lickfett L, Mahesh M, Vasamreddy C, et al. Radiation exposure during catheter ablation of atrial fibrillation. Circulation 2004;110:3003–10.
28. Efstathopoulos EP, Katritsis DG, Kottou S, et al. Patient and staff radiation dosimetry during cardiac electrophysiology studies and catheter ablation procedures: a comprehensive analysis. Europace 2006;8:443–8.
29. Achenbach S, Marwan M, Ropers D, et al. Coronary computed tomography angiography with a consistent dose below 1 mSv using prospectively electrocardiogram-triggered high-pitch spiral acquisition. Eur Heart J 2010;31:340–6.

Key Words: arrhythmia ■ C-arm computed tomography ■ catheter ablation ■ computed tomography ■ electrophysiology ■ imaging.